

Robust Multi-Objective Beamforming for Integrated Satellite and High Altitude Platform Network With Imperfect Channel State Information

Zhi Lin^{ID}, Min Lin^{ID}, Member, IEEE, Yongming Huang^{ID}, Senior Member, IEEE,
Tomaso de Cola^{ID}, Member, IEEE, and Wei-Ping Zhu^{ID}, Senior Member, IEEE

Abstract—In this paper, we propose a robust beamforming (BF) scheme for an integrated satellite and high altitude platform network, where a multibeam satellite system shares the millimeter wave spectrum with a high altitude platform system. Specifically, we first exploit the weighted Tchebycheff method and formulate a multi-objective optimization problem to obtain the Pareto optimal trade-off between two conflicting yet desirable objectives, namely, sum rate maximization and total transmit power minimization, while satisfying the quality-of-service constraints of both earth stations and mobile terminals and per-antenna transmit power budget. Then, by using the angular information based imperfect channel state information, we propose a low-complexity discretization method to transform the non-convex objective function and constraints to the convex ones. Furthermore, a monotonic optimization scheme combined with iterative penalty function algorithm is presented to obtain the BF weight vectors with low computational complexity and fast convergence rate. Finally, numerical results are provided to confirm the effectiveness and superiority of the proposed approach in comparison to the existing related works.

Index Terms—Integrated satellite and high altitude platform network, millimeter wave, multi-objective optimization, robust beamforming.

I. INTRODUCTION

HIGH altitude platform (HAP) has been used as an aerial base station to provide a fast-deployable services for

Manuscript received May 28, 2019; revised September 25, 2019; accepted October 11, 2019. Date of publication November 6, 2019; date of current version December 11, 2019. The associate editor coordinating the review of this manuscript and approving it for publication was Prof. Marco Moretti. This work was supported by the Key International Cooperation Research Project under Grant 61720106003. (*Corresponding author: Min Lin.*)

Z. Lin is with the College of Communications Engineering, Army Engineering University of PLA, Nanjing 210007, China, and also with the Department of Electrical and Computer Engineering, McGill University, Montreal, QC H3A 0G4, Canada (e-mail: linzhi945@163.com).

M. Lin is with the School of Communication and Information Engineering, Nanjing University of Posts and Telecommunications, Nanjing 210003, China (e-mail: linmin@njupt.edu.cn).

Y. Huang is with the National Mobile Communications Research Laboratory, Southeast University, Nanjing 210096, China (e-mail: huangym@seu.edu.cn).

T. de Cola is with the Institute of Communications and Navigation, German Aerospace Center, 82234 Oberpfaffenhofen, Germany (e-mail: tomaso.decola@dlr.de).

W.-P. Zhu is with the Department of Electrical and Computer Engineering, Concordia University, Montreal, QC H3G 1M8 Canada, and also with the School of Communication and Information Engineering, Nanjing University of Posts and Telecommunications, Nanjing 210003, China (e-mail: weiping@ece.concordia.ca).

Digital Object Identifier 10.1109/TSP.2019.2952045

hot-spot areas (e.g. vocal concerts or Olympic games) or data services for remote geographic areas [1], [2]. Due to the nature of a quasi-stationary position in the stratosphere, HAP has a large footprint for providing services over wide regions with low traffic cost [3]. Compared to terrestrial wireless networks, HAP communication is subject to low scattering and multi-path effects and thus offers a reliable transmission for users in remote, rural areas in contrast to a multi-cell infrastructure. As compared to satellite communication (SATCOM), on the other hand, HAP communication enjoys lower transmission delay as well as lower cost operation [4]. Besides the above advantages, HAP is also well-known due to its flexibility of deployment, high elevation angles, broad coverage, and easy mobility in emergency situations, etc. The seamless interoperability between various networks is expected to strengthen the foundation for 5G wireless system and beyond [5]. In this context, the application of HAP provides an excellent design option for future wireless communications. The utilization of HAP as new radio access platform for the 5G wireless communication system has been considered by the 3GPP [6].

A. Previous Works

International telecommunication union (ITU) recommended the frequency range between 18–32 GHz be one of the spectrum candidates for the HAP communication [7]. However, part of this band has already been allocated to SATCOM in Ka band [8]. In this regard, the framework of integrated satellite and HAP network (ISHAPN) is proposed to efficiently realize spectrum resource management, coordination and inter-operability between HAPs and satellites (SAT), which has been adopted in ABSOLUTE project [9]. Besides, the framework of ISHAPN has also been introduced in academia [10]. However, one of the urgent issue with ISHAPN is the mutual interference. In this context, the beamforming (BF) techniques in [11]–[13] are capable of enhancing the received signal quality at the intended user and suppressing signal leakage to the unintended user, and has been widely used in satellite/HAP fields to realize interference management [14]–[17]. For instance, the authors of [14] addressed the achievable secrecy rate maximization problem by jointly designing both the cooperative and non-cooperative BF schemes under power budget and quality-of-service (QoS) constraints in satellite-terrestrial network (STN). By exploiting BF technique to realize interference alignment, a novel method

1053-587X © 2019 IEEE. Personal use is permitted, but republication/redistribution requires IEEE permission.
See http://www.ieee.org/publications_standards/publications/rights/index.html for more information.

was proposed in [15] for achieving the maximum sum rate in HAP-based communications. In [16], the authors proposed intelligent BF strategies to enhance the coverage and capacity of HAP communications. Besides, a low-complexity location-assisted BF scheme was investigated to improve the spectral efficiency in HAP downlink communications in [17].

In the above-mentioned works, it is assumed that the channel state informations (CSIs) of all links are perfectly known. However, due to the mobility of terminals, estimation mismatch and/or feedback errors, it is almost impossible to obtain the perfect CSI [18]–[20]. Therefore, robust BF design based on imperfect CSI has received more attention recently [21]. Among the existing robust BF design, three kinds of channel uncertainty models, namely, deterministic uncertainty model [22], [23], stochastic uncertainty model [24], [25] and angular information based uncertainty model [26]–[28] are commonly used. The deterministic uncertainty model, which assumes that the actual CSI lies in the uncertainty set or region, is suitable to characterize instantaneous CSI with errors. In [22], Huang and Swindlehurst proposed a robust transmission BF design in multiple-input single-output (MISO) wiretap channels, where channel errors laid in a bounded uncertainty region. The stochastic uncertainty model assumes that the CSI is randomly distributed and its statistics are known at the transmitter. Under this assumption, by adopting a stochastic model for the CSI uncertainty, the authors in [24] investigated a robust secure BF framework to minimize the transmit power, while satisfying secrecy constraints and QoS requirements. Ma *et al.* in [25] proposed a robust BF design to improve system performance under the transmit power constraint for both spherical uncertainty and statistical CSI. The angular information based uncertainty model, which assumes the channel estimation includes imperfect angular information (e.g., degree of arrival/departure DoA/DoD), has low scattering effect and is suitable for high spectral band. Thus, how to design robust scheme by exploring the angular information based uncertainty model becomes an significative direction in mmWave communication scenarios. Xu *et al.* in [27] investigated the three-dimensional (3D) massive multiple-input multiple-output (MIMO) for air-to-ground transmission with the imperfect AoD uncertainty assumption. The authors in [28] proposed a channel uncertainty model based on imperfect DoA information, and investigated the robust BF design to improve system performance in STN.

Next generation wireless networks aim at providing diverse services, including higher transmission rates, wider communication coverage, higher reliability and lower latency, lower energy consumption and so on [29]. Motivated by this fact, the multi-objective optimization (MOO), which simultaneously satisfies multiple objectives, has attracted much attention recently (e.g., see [30] and the references there in). For example, in [31], the MOO problem was studied in full-duplex wireless communication systems to investigate the trade-off between total downlink and uplink transmit power minimization, where the semidefinite programming relaxation was adopted to obtain the optimal solutions. The authors in [32] proposed a MOO framework for multiuser MISO secondary communication systems. In [33], three critical issues, i.e., signal transmission, energy and security were investigated in MIMO interference networks by using the

modified weighted Tchebycheff method. It is worth-mentioning that most of existing MOO researches focused on optimization with available CSI, which is not realistic.

B. Motivations and Contributions

In this paper, we investigate the trade-off between two conflicting yet desirable objectives, namely, sum rate maximization and total transmit power minimization in ISHAPN with angular information based imperfect CSI. To the best of our knowledge, the robust MOO beamforming design with angular information based imperfect CSI is still a new yet challenging topic in ISHAPN related fields, and so far no research work has been published. These observations motivate our work in this paper.

The contributions of this paper are summarized as follows:

- We model the satellite and HAP channels with the aid of standard recommendations, and develop an analytical framework for the ISHAPN, where the satellite is equipped with multibeam antenna with array-fed reflectors while the HAP employs uniform planar array (UPA). Based on the framework, the joint optimization design arises so that these two systems can share spectrum resource and cooperate with each other.
- By using the weighted Tchebycheff method, we formulate a MOO problem to optimize the sum rate maximization and total transmit power minimization, while satisfying the QoS requirements of the earth stations (ESs) and mobile terminals (MTs), and per-antenna transmit power budget. To the best of our knowledge, the MOO problem in realizing spectral coexistence between satellite network and other wireless networks is new as none of the previous related works addressed this issue and most of existing schemes were designed for single objective optimization, e.g. [34] aiming at achievable secrecy rate maximization and [16], [27] focusing on improving spectral efficiency. Beside, the Pareto optimal trade-off between the two objectives can be obtained through the proposed method.
- Since the formulated MOO problem is non-convex and mathematically intractable, we first exploit angular information based imperfect CSI and propose a discretization method to transform the original optimization problem into convex one. Then, a novel monotonic optimization scheme combining with iterative penalty function (IPF) algorithm is presented to solve the problem and obtain the optimal BF weight vectors. It is worth-mentioning that here we utilize the angular information to implement the robust BF design, thus the proposed scheme is more practical than those focusing on MOO problem with perfect CSI assumption [31], [33].

The rest of this paper is organized as follows. Section II introduces the system model and channel model. The MOO problem is formulated in Section III. In Section IV, the monotonic optimization scheme, including the discretization method and iterative penalty function algorithm, is proposed. In Section V, simulation results are provided together with discussions. Finally, we conclude our paper in Section VI.

Notation: Bold uppercase and lowercase letters denote matrices and vectors, respectively. $(\cdot)^T$, $(\cdot)^H$, $\text{Tr}(\cdot)$ and $\text{rank}(\cdot)$

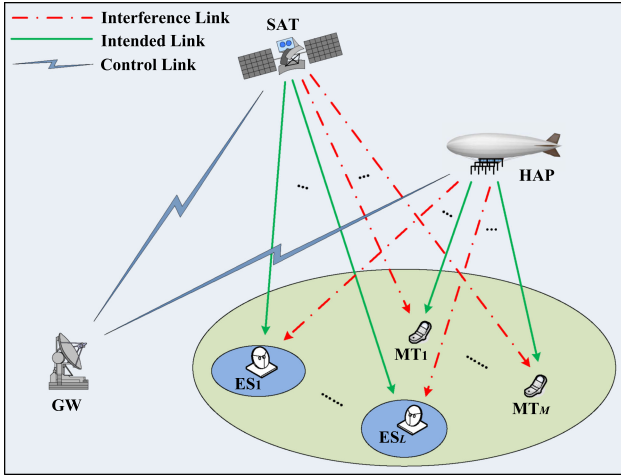


Fig. 1. System model of the considered ISHAPN.

stand for the transpose, Hermitian transpose, trace and rank of a matrix. $\|\cdot\|$ and $|\cdot|$ denote Euclidean norm and absolute value of a vector. $\mathbb{C}^{M \times N}$ denotes the complex space of $M \times N$, \mathbf{I}_N the $N \times N$ identity matrix. \mathbb{R}_+ denotes the real number set. $\mathbf{X} \succeq \mathbf{0}$ means that matrix \mathbf{X} is a positive semi-definite matrix. $\mathbf{X} \leq \mathbf{Y}$ means each element of \mathbf{Y} is not less than that of \mathbf{X} . $\mathbf{X} \odot \mathbf{Y}$ and $\mathbf{X} \otimes \mathbf{Y}$ denote Hadamard and Kronecker product of matrices \mathbf{X} and \mathbf{Y} , respectively, $\langle \mathbf{X}, \mathbf{Y} \rangle = \text{Tr}(\mathbf{X}^H \mathbf{Y})$, $\log(\cdot)$ the natural logarithm, $\mathcal{CN}(\mu, \sigma^2)$ the complex Gaussian distribution with mean μ and variance σ^2 .

II. SYSTEM AND CHANNEL MODEL

As shown in Fig. 1, we consider the downlink transmission of an ISHAPN, where the geostationary orbit (GEO) satellite serves L ESSs through multicast communication, while the HAP acts like aerial base station to provide data connections to M MTs. In this configuration, it is assumed that the satellite is equipped with N_s directional antennas, the HAP with N_a UPA antennas to achieve high gain with compact size, and the whole system operates at mmWave band. Here, the gateway acts as a control center to manage the whole network to collect and manage various kinds of information, such as the CSI of all links, the QoS requirement, and implement the control function, like resource allocation. In addition, the frequency flat slow fading channel is adopted and only the angular information based imperfect CSI is known at the gateway due to the channel estimation error and feedback delay [35].

A. Satellite Downlink Channel Model

In this paper, the satellite employs array fed reflector antenna with N_s feeds uniformly placed along a circle with radius d , which is shown in Fig. 2. By considering the effects of path loss, rain attenuation and satellite beam gain, the geometry based 3D mmWave satellite downlink channel between the SAT and any user (ES or MT) can be expressed as [36]

$$\mathbf{f} = \sqrt{C_L G_R / \xi} \mathbf{b}_g(\phi, \psi) \odot \mathbf{a}_c(\phi, \psi) \quad (1)$$

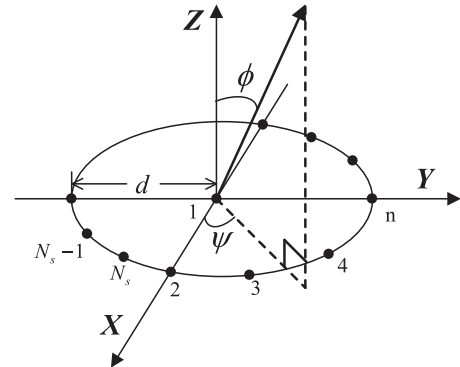


Fig. 2. Geometrical model of on-board feed array.

where C_L denotes the path loss coefficient, which can be calculated as

$$C_L = \left(\frac{\lambda}{4\pi} \right)^2 \frac{1}{d_h^2 + d_0^2} \quad (2)$$

where λ denotes the wavelength, $d_h \approx 35786$ km the height of GEO satellite, d_0 the distance from beam center to the center of central beam. In addition, ξ in (1) represents the rain attenuation effect. The power gain in dB, $\xi_{\text{dB}} = 20 \log_{10}(\xi)$, commonly follows lognormal random distribution $\ln(\xi_{\text{dB}}) \sim \mathcal{CN}(\mu, \sigma^2)$. Besides, $\mathbf{b}_g(\phi, \psi)$ denotes the beam gain at satellite antenna feeds, with $\phi \in [0, \pi/2]$ and $\psi \in [0, 2\pi)$ being the elevation angle and the azimuth angle. Since the beam coverage area generated by multibeam satellite is related with corresponding antenna feed, the n -th element of $\mathbf{b}_g(\phi, \psi)$ can be expressed as [36]

$$b_n(\phi, \psi) = \sqrt{\eta} \frac{\pi D}{\lambda} \frac{J_1(u_n)}{u_n} \quad (3)$$

where η denotes the antenna efficiency, D the antenna feed diameter, $J_1(\cdot)$ the first-kind Bessel function of order 1, and u_n can be expressed as

$$u_n = \frac{\pi D}{\lambda} \sin \left(\sqrt{(\phi - \phi_n)^2 + (\psi - \psi_n)^2} \right) \quad (4)$$

with (ϕ_n, ψ_n) being the center direction of the n -th beam. For the array steering vector (SV) $\mathbf{a}(\phi, \psi)$ in (1), by denoting $\beta = 2\pi/\lambda$, the phase delay of the n -th element (except for the center element) with respect to the center in the uniform circular array (UCA) can be computed as [37]

$$\tau_n = \beta d \sin \phi \cos \left(\frac{2\pi(n-2)}{N_s-1} - \psi \right), \quad n \in \{2, \dots, N_s\}. \quad (5)$$

Thus, the SV can be expressed as

$$\begin{aligned} \mathbf{a}_c(\phi, \psi) \\ = \left[1, e^{j\beta d \sin \phi \cos(-\psi)}, \dots, e^{j\beta d \sin \phi \cos(\frac{2\pi(N_s-2)}{N_s-1} - \psi)} \right]^T. \end{aligned} \quad (6)$$

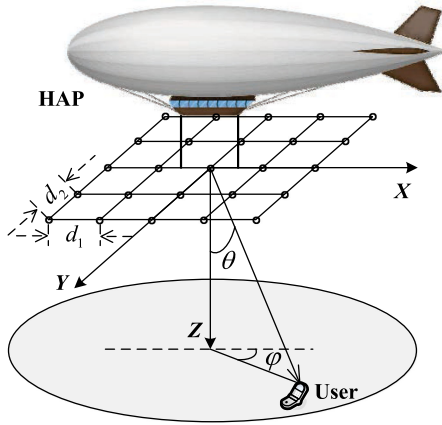


Fig. 3. Geometrical relation between HAP and any user.

In addition, $G_R = 10^{\tilde{G}_R/10}$ with \tilde{G}_R denoting the ES off-boresight antenna gain pattern in dB as given by [38].

$$\tilde{G}_r(v) = \begin{cases} G_{\max} - 2.5 \times 10^{-3} \left(\frac{D}{\lambda} v \right)^2, & 0^\circ < v < v_m \\ 2 + 15 \log \frac{D}{\lambda}, & v_m \leq v < v_r \\ 32 - 25 \log v, & v_r \leq v < 48^\circ \\ -10, & 48^\circ \leq v \leq 180^\circ \end{cases}$$

where G_{\max} denotes maximal gain of the ES antenna, v the off-boresight angle, $v_m = \frac{20\lambda}{D} \sqrt{G_{\max} - (2 + 15 \log \frac{D}{\lambda})}$ and $v_r = 15.85(\frac{D}{\lambda})^{-0.6}$ in degrees.

B. HAP Downlink Channel Model

As illustrated in Fig. 3, we assume that HAP employs UPA of dimension $N_a = N_1 \times N_2$ to achieve high gain with compact size. Due to the highly directional and quasi-optical nature of the radio wave propagation at high frequency band, the HAP downlink channel can be considered as a superposition of a predominant line-of-sight (LoS) propagation component and a sparse set of single-bounce non-LoS (NLoS) components. Mathematically, the HAP downlink channel matrix can be expressed as [27]

$$\mathbf{H} = \sqrt{g_e(\theta_0, \varphi_0)} \rho_0 \mathbf{A}(\theta_0, \varphi_0) + \sqrt{\frac{1}{L_n}} \sum_{i=1}^{L_n} \sqrt{g_e(\theta_i, \varphi_i)} \rho_i \mathbf{A}(\theta_i, \varphi_i) \quad (7)$$

where L_n is the number of NLoS paths, $\rho_i (i = 0, 1, \dots, L_n)$ represents the complex channel gain associated with the i -th path. The path loss of the LoS component in dB can be calculated as (2). The recent measurements revealed that the amplitudes of the NLoS components, namely $|\rho_i|^2$, ($i = 1, \dots, L_n$) are typically 5 to 10 dB weaker than that of the LoS component $|\rho_0|^2$. In (7), $g_e(\theta, \varphi)$ denotes the element pattern with θ and φ being the horizontal and vertical DoA, respectively. According to the model introduced by ITU, the element pattern in dB, namely, $\hat{g}_e(\theta, \varphi) = 10 \log_{10}(g_e(\theta, \varphi))$ can be described as

$$\hat{g}_e(\theta, \varphi) = E_{\max} - \min \{g_x(\theta, \varphi) + g_y(\theta, \varphi), S_m\} \quad (8)$$

TABLE I
DESCRIPTION OF THE PARAMETERS

Parameter	Definition
L / M	number of ESs / MTs
N_s / N_a	antenna numbers of SAT / HAP
N_1 / N_2	number of array elements placed along the X/Y-axis
d_1 / d_2	inter-element spacing placed along the X/Y-axis
$\mathbf{f}_{s,l} / \mathbf{f}_{a,m}$	channel vector between SAT and l -th ES / m -th MT
$\mathbf{h}_{s,l} / \mathbf{h}_{a,m}$	channel vector between HAP and l -th ES / m -th MT
$\mathbf{w}_s / \mathbf{w}_m$	BF weight vector toward ESs / m -th MT
$\sigma_{s,l}^2 / \sigma_{a,m}^2$	noise variance at l -th ES / m -th MT
$\kappa / B / T$	Boltzmann constant / bandwidth / noise temperature

where E_{\max} denotes the maximum antenna gain, $g_x(\theta, \varphi)$ and $g_y(\theta, \varphi)$ the relative patterns in X and Y planes, respectively, given by [28]

$$\begin{aligned} g_x(\theta, \varphi) &= \min \left\{ 12 \left(\frac{\arctan(\cot \theta / \cos \varphi)}{\varphi_x^{3dB}} \right)^2, S_m \right\}, \\ g_y(\theta, \varphi) &= \min \left\{ 12 \left(\frac{\arctan(\tan \theta \sin \varphi)}{\varphi_y^{3dB}} \right)^2, S_m \right\} \end{aligned} \quad (9)$$

where φ_x^{3dB} and φ_y^{3dB} represent the 3 dB beamwidth of the X and Y patterns, respectively, S_m the side-lobe level of the antenna pattern.

By denoting $\mathbf{r}_{m,n} = [x_m, y_n, 0]^T$ as the location vector of (m, n) -th element and $\mathbf{d} = [\cos \varphi \sin \theta, \sin \varphi \sin \theta, \cos \theta]^T$ the DoA unit vector, the phase delay of the (m, n) -th element with respect to the center point is given by

$$\begin{aligned} \tau_{m,n} &= \beta \langle \mathbf{d} \cdot \mathbf{r}_{m,n} \rangle \\ &= \beta ((m - (N_1 + 1)/2) d_1 \sin \theta \cos \varphi \\ &\quad + (n - (N_2 + 1)/2) d_2 \sin \theta \sin \varphi). \end{aligned} \quad (10)$$

Thus, the (m, n) -th element of the array steering matrix can be expressed as

$$\begin{aligned} [\mathbf{a}(\theta, \varphi)]_{m,n} &= \exp(j\tau_{m,n}) \\ &= \exp[j\beta((m - (N_1 + 1)/2) d_1 \sin \theta \cos \varphi \\ &\quad + (n - (N_2 + 1)/2) d_2 \sin \theta \sin \varphi)]. \end{aligned} \quad (11)$$

And the array steering matrix can be reformulated as

$$\mathbf{A}(\theta, \varphi) = \mathbf{a}_x(\theta, \varphi) \mathbf{a}_y^H(\theta, \varphi) \quad (12)$$

where $\mathbf{a}_x(\theta, \varphi)$ and $\mathbf{a}_y(\theta, \varphi)$ denote the X and Y steering vectors of the UPA, which can be, respectively, written as

$$\begin{aligned} \mathbf{a}_x(\theta, \varphi) &= [e^{-j\beta((N_1 - 1)/2)d_1 \sin \theta \cos \varphi}, \dots, \\ &\quad e^{+j\beta((N_1 - 1)/2)d_1 \sin \theta \cos \varphi}]^T, \\ \mathbf{a}_y(\theta, \varphi) &= [e^{-j\beta((N_2 - 1)/2)d_2 \sin \theta \sin \varphi}, \dots, \\ &\quad e^{+j\beta((N_2 - 1)/2)d_2 \sin \theta \sin \varphi}]^T. \end{aligned} \quad (13)$$

Now, for the sake of simplicity, we transform the 3D channel matrix into vector form as

$$\begin{aligned} \mathbf{h} &= \sqrt{G_r(\theta)} \operatorname{vec}(\mathbf{H}) \\ &= \sqrt{G_r(\theta_0) g_e(\theta_0, \varphi_0)} \rho_0 \mathbf{a}_x(\theta_0, \varphi_0) \otimes \mathbf{a}_y(\theta_0, \varphi_0) \\ &\quad + \sqrt{\frac{1}{L_n}} \sum_{i=1}^{L_n} \sqrt{G_r(\theta_i) g_e(\theta_i, \varphi_i)} \rho_i \mathbf{a}_x(\theta_i, \varphi_i) \otimes \mathbf{a}_y(\theta_i, \varphi_i). \end{aligned} \quad (14)$$

Here, the antenna pattern $G_r(\theta)$ of HAP mobile terminal with respect to the relative angle θ to its boresight, is given by [7]

$$G_r(\theta) = \begin{cases} G_m 10^{-\frac{3}{10}(\frac{2\theta}{\omega})^2}, & |\theta| \leq \frac{\theta_m}{2}, \\ G_s, & \frac{\theta_m}{2} \leq |\theta| \leq \pi \end{cases} \quad (15)$$

where ω denotes the half-power (3 dB) beamwidth and θ_m is the main-lobe beamwidth. G_m and G_s represent the maximum main-lobe gain and averaged side-lobe gain, respectively.

Considering the high directionality of mmWave channel and channel error (including estimation error, feedback delay, and mobility of ground users), we suppose that both the HAP and satellite downlink channels belong to given uncertainty sets Δ , and the sets are available at transmitters. Specifically, the precise position of MT is unknown but the uncertainty region based on angular information where it is located known to be $\Delta = \{\theta_i \in [\theta_{i,Lo}, \theta_{i,Up}], \varphi_i \in [\varphi_{i,Lo}, \varphi_{i,Up}]\}$ (i is the index for MTs), which is also applicable to the satellite downlink channels, after replacing θ and φ with ϕ and ψ . It should be mentioned that the uncertainty model stands for possible range of LoS component instead of the NLoS components.

III. PROBLEM FORMULATION

Suppose that the SAT transmits common signal $s(t)$, satisfying $E[|s(t)|^2] = 1$, which is mapped onto the UCA with BF weight vector $\mathbf{w}_s \in \mathbb{C}^{N_s \times 1}$ before transmission. Meanwhile, the HAP sends signal $x_m(t)$ with normalized power to the m -th MT, also mapped onto the UPA with BF weight vector $\mathbf{w}_m \in \mathbb{C}^{N_a \times 1}$. Thus, the received signals at the l -th ES and m -th MT are, respectively, given by

$$y_{s,l}(t) = \mathbf{f}_{s,l}^H \mathbf{w}_s s(t) + \sum_{m=1}^M \mathbf{h}_{s,l}^H \mathbf{w}_m x_m(t) + n_{s,l}(t), \quad (16a)$$

$$\begin{aligned} y_{a,m}(t) &= \mathbf{h}_{a,m}^H \mathbf{w}_m x_m(t) + \sum_{i=1, i \neq m}^M \mathbf{h}_{a,m}^H \mathbf{w}_i x_i(t) \\ &\quad + \mathbf{f}_{a,m}^H \mathbf{w}_s s(t) + n_{a,m}(t) \end{aligned} \quad (16b)$$

where $n_{s,l}(t) \sim \mathcal{CN}(0, \sigma_{s,l}^2)$ and $n_{a,m}(t) \sim \mathcal{CN}(0, \sigma_{a,m}^2)$ denotes i.i.d. additive white Gaussian noise, where $\sigma_i^2 = \kappa B T, i \in \{(s, l), (a, m)\}$. According to (16), the received SINR at l -th ES and m -th MT can be described as

$$\begin{aligned} \gamma_{s,l} &= \frac{|\mathbf{f}_{s,l}^H \mathbf{w}_s|^2}{\sum_{m=1}^M |\mathbf{h}_{s,l}^H \mathbf{w}_m|^2 + \sigma_{s,l}^2}, \\ \gamma_{a,m} &= \frac{|\mathbf{h}_{a,m}^H \mathbf{w}_m|^2}{\sum_{i=1, i \neq m}^M |\mathbf{h}_{a,m}^H \mathbf{w}_i|^2 + |\mathbf{f}_{a,m}^H \mathbf{w}_s|^2 + \sigma_{a,m}^2}. \end{aligned} \quad (17)$$

Then, the achievable rate of the l -th ES and the m -th MT are thus given by

$$\begin{aligned} R_{s,l} &= \log_2 (1 + \gamma_{s,l}), \\ R_{a,m} &= \log_2 (1 + \gamma_{a,m}). \end{aligned} \quad (18)$$

Based on (18), we first investigate the worst-case sum rate maximization problem, which is given by

P1 (Worst-Case Sum Rate Maximization):

$$\begin{aligned} &\max_{\mathbf{w}_s, \mathbf{w}_m} \min_{\Delta} \sum_{l=1}^L \alpha_{s,l} R_{s,l} + \sum_{m=1}^M \alpha_{a,m} R_{a,m} \\ &\text{s.t. C1: } \min_{\Delta} \gamma_{a,m} \geq \Gamma_{a,m}, \quad \forall m, \\ &\quad \text{C2: } \min_{\Delta} \gamma_{s,l} \geq \Gamma_{s,l}, \quad \forall l, \\ &\quad \text{C3: } \sum_{m=1}^M [\mathbf{w}_m]_i^2 \leq P_{a,i}, \quad \forall i, \\ &\quad \text{C4: } [\mathbf{w}_s]_j^2 \leq P_{s,j}, \quad \forall j \end{aligned} \quad (19)$$

where $\alpha_{s,l}$ and $\alpha_{a,m}$ are non-negative constant weight for $R_{s,l}$ and $R_{a,m}$, respectively, under the constraint $\sum_{l=1}^L \alpha_{s,l} + \sum_{m=1}^M \alpha_{a,m} = 1$, $\Gamma_{a,m}$ and $\Gamma_{s,l}$ denote the SINR constraints of m -th MT and l -th ES, respectively, $P_{a,i}$ and $P_{s,j}$ the per-antenna power budget at i -th and j -th antenna feed of HAP and satellite, respectively. The constraints C1 and C2 represent the required SINR of m -th MT and l -th ES, while the constraints C3 and C4 represent the per-antenna power budget. In practical wireless networks, each transmit antenna is assigned an individual power amplifier in its analog front-end, we thus take the per-antenna power constraints of satellite and base station into account, which is more realistic than the commonly used total power constraints [14], [28].

The second system objective is the minimization of total transmit power at both satellite and HAP, which can be mathematically formulated as

P2 (Total Transmit Power Minimization):

$$\begin{aligned} &\min_{\mathbf{w}_s, \mathbf{w}_m} \sum_{m=1}^M \|\mathbf{w}_m\|^2 + \|\mathbf{w}_s\|^2 \\ &\text{s.t. C1-C4.} \end{aligned} \quad (20)$$

Generally speaking, a higher sum rate achievement needs a higher transmit power consumption [39], [40]. Equivalently, based on the conservation of energy theorem, the less transmit power consumed at transmitter would also lead to lower system sum rate. Thus, the objectives of P1 and P2 conflicts with each other. To resolve it, we propose a non-trivial trade-off design for balancing two conflicting objectives through investigating multi-objective problem.

By applying Pareto optimality and weighted Tchebycheff method [32], the MOO problem can be formulated as

P3 (Multi-Objective Optimization):

$$\begin{aligned} &\min_{\mathbf{w}_s, \mathbf{w}_m} \max_{\Delta, n \in \{1, 2\}} \{\lambda_n (f_n(\mathbf{w}_s, \mathbf{w}_m) - f_n^*)\} \\ &\text{s.t. C1-C4} \end{aligned} \quad (21)$$

where $f_1(\mathbf{w}_s, \mathbf{w}_m) = -(\sum_{l=1}^L \alpha_{s,l} R_{s,l} + \sum_{m=1}^M \alpha_{a,l} R_{a,l})$, $f_2(\mathbf{w}_s, \mathbf{w}_m) = \sum_{m=1}^M \|\mathbf{w}_m\|^2 + \|\mathbf{w}_s\|^2$, f_n^* is the optimal objective value of the n -th problem and treated as a constant for P3. Besides, λ_n denotes the weighted factor which represents the priority level of the n -th problem from a systematic perspective under the constraint $\lambda_1 + \lambda_2 = 1$. By varying λ_n , we can obtain a complete Pareto optimal set which corresponds to a set of preference policies among sum rate and power consumption.

Remark 1: Compared with other scalarization methods for achieving the Pareto optimality of MOO problem (e.g. the exponentially weighted method and ε -constraint method), the weighted Tchebycheff method can achieve the complete Pareto optimal set with a lower computational complexity. It can be also observed that when $\lambda_1 = 1$, P3 is transformed into P1. Similarly, P3 is equivalent with P2 when $\lambda_2 = 1$.

IV. PROPOSED ROBUST BEAMFORMING SCHEMES

We note that P1 and P3 are non-convex due to the non-convex objectives. Besides, the constraints C1 and C2 involve infinite inequality constraints due to the continuity of the corresponding CSI uncertainty sets, which make P3 very difficult to solve directly. To overcome this predicament, we first transform C1 and C2 into tractable forms. Then, the optimal objective values f_1^* of P1 and f_2^* of P2 are obtained by monotonic optimization scheme and iterative penalty function approach. Finally, the MOO problem can be efficiently solved through similar methods used for solving P1 and P2.

It can be found that both the constraints C1 and C2 on uncertainty region Δ are non-convex, coupled and difficult to solve. To address this problem, a discretization method is proposed to discretize the channel uncertainty region in (19). We first discuss the discrete uncertainty Δ_d which contains discrete elements, i.e.,

$$\Delta_d = \{\mathbf{h}_1, \dots, \mathbf{h}_N\} \quad (22)$$

where \mathbf{h}_n denotes possible channel in uncertainty Δ_d , N the discrete sample number. The discrete uncertainty is the most general form since any uncertainty shape can be expressed as either finite or infinite discrete points. Then, the discrete uncertainty of channel matrix can be expressed as

$$\Omega = \{\mathbf{h}_1 \mathbf{h}_1^H, \dots, \mathbf{h}_N \mathbf{h}_N^H\}. \quad (23)$$

Thus, any channel matrix in uncertainty set can be represented as the combination of the discrete points in (23). Since only the uncertainty region based on angular information is known, we select uniformly spaced angles in the set of Ω

$$\begin{aligned} \theta^{(i)} &= \theta_{Lo} + (i-1)\Delta_\theta, \quad i = 1, \dots, M_1, \\ \varphi^{(j)} &= \varphi_{Lo} + (j-1)\Delta_\varphi, \quad j = 1, \dots, M_2 \end{aligned} \quad (24)$$

where $\theta^{(i)}$ and $\varphi^{(j)}$ are the LoS angular information of $\mathbf{h}^{(i,j)}$, $M_1 \geq N_1$ and $M_2 \geq N_2$ represent number of samples on θ and φ , and $\Delta_\theta = (\theta_U - \theta_L)/(M_1 - 1)$, $\Delta_\varphi = (\varphi_U - \varphi_L)/(M_2 - 1)$. The above formulation is also suitable for ϕ and ψ in satellite downlink channel, which is omitted for simplicity. We denote $\mathbf{W}_s = \mathbf{w}_s \mathbf{w}_s^H$, $\mathbf{W}_m =$

$\mathbf{w}_m \mathbf{w}_m^H$, and define $\tilde{\mathbf{H}} = \sum_{i=1}^{M_1} \sum_{j=1}^{M_2} \mu_{i,j} \mathbf{H}^{(i,j)}$ and $\tilde{\mathbf{F}} = \sum_{i=1}^{M_1} \sum_{j=1}^{M_2} \mu_{i,j} \mathbf{F}^{(i,j)}$, where $\mathbf{H}^{(i,j)} = \mathbf{h}^{(i,j)} (\mathbf{h}^{(i,j)})^H$ and $\mathbf{F}^{(i,j)} = \mathbf{f}^{(i,j)} (\mathbf{f}^{(i,j)})^H$. Here, we assume $\mu_{i,j} = \frac{1}{M_1 M_2}$, which has been adopted in [26] with satisfied robustness. Thus, \min_{Δ} of the objective in P1 can be removed, and the constraints C1 and C2 can be expressed as the following convex inequality constraints

$$\begin{aligned} \text{Tr}(\tilde{\mathbf{H}}_{a,m} \mathbf{W}_m) - \Gamma_{a,m} \left(\sum_{i=1, i \neq m}^M \text{Tr}(\tilde{\mathbf{H}}_{a,m} \mathbf{W}_i) \right. \\ \left. + \text{Tr}(\tilde{\mathbf{F}}_{a,m} \mathbf{W}_s) \right) \geq \Gamma_{a,m} \sigma_{a,m}^2, \quad \forall m, \end{aligned} \quad (25a)$$

$$\text{Tr}(\tilde{\mathbf{F}}_{s,l} \mathbf{W}_s) - \Gamma_{s,l} \left(\sum_{m=1}^M \text{Tr}(\tilde{\mathbf{H}}_{s,l} \mathbf{W}_m) \right) \geq \Gamma_{s,l} \sigma_{s,l}^2, \quad \forall l. \quad (25b)$$

Then we focus on solving P1, a novel monotonic optimization approach is adopted to solve P1 to obtain optimal value f_1^* . This method is to directly search for the optimal value set of $R_{s,l}$ and $R_{a,m}$ through constructing a set of overlapping boxes which maintain the achievable region, where the optimal solution lies in, and the coverage of boxes iteratively decrease until the optimal solution is obtained. Thus, we define the variables $\mathbf{r} = \{r_{s,1}, \dots, r_{s,L}, r_{a,1}, \dots, r_{a,M}\}$ to represent achievable rate of ESs and MTs, and rewrite P1 as

$$\begin{aligned} \max_{\mathbf{W}_s, \mathbf{W}_m, r_{s,l}, r_{a,m}} g(\mathbf{r}) : & \sum_{l=1}^L \alpha_{s,l} r_{s,l} + \sum_{m=1}^M \alpha_{a,m} r_{a,m} \\ \text{s.t. } \tilde{\text{C1}}: & \text{Tr}(\tilde{\mathbf{H}}_{a,m} \mathbf{W}_m) - \hat{r}_{a,m} \left(\sum_{i=1, i \neq m}^M \text{Tr}(\tilde{\mathbf{H}}_{a,m} \mathbf{W}_i) \right. \\ & \left. + \text{Tr}(\tilde{\mathbf{F}}_{s,l} \mathbf{W}_s) \right) \geq \hat{r}_{a,m} \sigma_{a,m}^2, \quad \forall m, \\ \tilde{\text{C2}}: & \text{Tr}(\tilde{\mathbf{F}}_{s,l} \mathbf{W}_s) - \hat{r}_{a,m} \sum_{m=1}^M \text{Tr}(\tilde{\mathbf{H}}_{s,l} \mathbf{W}_m) \\ & \geq \hat{r}_{a,m} \sigma_{a,m}^2, \quad \forall l, \\ \tilde{\text{C3}}: & \sum_{m=1}^M \text{diag}[\mathbf{W}_m]_i \leq P_{a,i}, \quad \forall i, \\ \tilde{\text{C4}}: & \text{diag}[\mathbf{W}_s]_i \leq P_{s,j}, \quad \forall j. \\ \tilde{\text{C5}}: & \text{rank}(\mathbf{W}_m) = \text{rank}(\mathbf{W}_s) = 1, \quad \forall m \end{aligned} \quad (26)$$

where $g(\mathbf{r})$ denotes the objective function of \mathbf{r} , $\hat{r}_{a,m} = \max(\Gamma_{a,m}, r_{a,m})$, $\hat{r}_{s,l} = \max(\Gamma_{s,l}, r_{s,l})$.

Then, the monotonic optimization scheme is adopted to obtain the optimal achievable rate in problem (26). We define the box as following.

Definition 1: For given $\mathbf{a}, \mathbf{b} \in \mathbb{R}_+^{M+L}$ with $\mathbf{a} \leq \mathbf{b}$, all the set of \mathbf{x} such that $\mathbf{a} \leq \mathbf{x} \leq \mathbf{b}$ is defined as a box $[\mathbf{a}, \mathbf{b}]$.

We initialize a box set $\mathbb{S} = [\mathbf{0}, \mathbf{b}_0]$, the elements of the upper bound \mathbf{b}_0 can be defined as maximal rate of each user in $\{R_{s,1}, \dots, R_{s,L}, R_{a,1}, \dots, R_{a,M}\}$ obtained by switching off HAP/satellite and letting satellite/HAP only serves the l -th/ m -th user with maximum transmit power, which can be calculated as $\log_2(1 + \sum_{j=1}^{N_s} P_{s,j} \|\mathbf{h}_{s,l}\|^2 / \sigma_{s,l}^2)$ or $\log_2(1 + \sum_{i=1}^{N_a} P_{a,i} \|\mathbf{h}_{a,m}\|^2 / \sigma_{a,m}^2)$. Thus, the initial upper and lower bounds of objective of P1 are written by $g_{\max} = g(\mathbf{b}_0)$ and $g_{\min} = g(\mathbf{a}_0)$, where the elements of the lower bound \mathbf{a}_0 can be calculated as the SINR threshold in $\tilde{\mathcal{C}}1$ and $\tilde{\mathcal{C}}2$, which is given by $\log_2(1 + \Gamma_{s,l})$ or $\log_2(1 + \Gamma_{a,m})$.

During each iteration, we select a box $[\mathbf{a}, \mathbf{b}]$ from \mathbb{S} satisfying $g(\mathbf{b}) = g_{\max}$, then check the feasibility of \mathbf{a} . If \mathbf{a} is not located among the achievable region of P1, then the box does not maintain feasible solution and can be directly removed from \mathbb{S} . Thus the box \mathbb{S} is updated as $\mathbb{S} = \mathbb{S} \setminus [\mathbf{a}, \mathbf{b}]$, and the upper bound of objective is reset as maximal value of updated box,

$$g_{\max} = \max_{\mathbb{S}} g(\mathbf{b}). \quad (27)$$

If \mathbf{a} is feasible in P1, we define l_{ab} as the line between \mathbf{a} and \mathbf{b} . To efficiently increase the lower bound of the box, a novel searching method is proposed to check the feasibility of point \mathbf{p} , which is the intersection point of the hyperplane $\{\mathbf{p} | g(\mathbf{p}) = g_{\min}\}$ and line l_{ab}

$$\mathbf{c} = \mathbf{a} + (\mathbf{b} - \mathbf{a}) \cdot \frac{g_{\min} - g(\mathbf{a})}{g(\mathbf{b} - \mathbf{a})}. \quad (28)$$

Since \mathbf{c} satisfies $g(\mathbf{c}) = g_{\min}$ and each element also meets the constraints of $\tilde{\mathcal{C}}1$ and $\tilde{\mathcal{C}}2$, \mathbf{c} is always feasible to P1, then the bisection method is conducted along line l_{cb} to obtain the intersection point on the Pareto boundary, giving the searching result \mathbf{p} and the lower bound $g_{\min} = g(\mathbf{p})$.

Next, the box $[\mathbf{a}, \mathbf{b}]$ is divided into $L + M$ non-overlapping boxes to improve the upper bound. Based on point \mathbf{p} , the upper vertices of i -th box in $\{\mathbf{b}^{(1)}, \dots, \mathbf{b}^{(L+M)}\}$ can be expressed as

$$\mathbf{b}^{(i)} = \mathbf{b} - (b_i - p_i) \mathbf{e}_i, \quad i = 1, \dots, L + M \quad (29)$$

where b_i and p_i represent the i -th element of \mathbf{b} and that of \mathbf{p} , respectively, and \mathbf{e}_i is a vector whose i -th element is 1 and the rest are 0. Thus the K upper vertices of i -th divided box can be written as $\{\mathbf{b}_1^{(i)}, \dots, \mathbf{b}_{L+M}^{(i)}\}$. Then, the corresponding lower vertices are calculated as

$$\mathbf{a}^{(i)} = \begin{cases} \mathbf{a}, & i = 1 \\ \mathbf{a}^{(i-1)} + (p_{i-1} - a_{i-1}) \mathbf{e}_{i-1}, & i > 1 \end{cases} \quad (30)$$

Since the intersection point \mathbf{p} is close to the Pareto boundary, the dividing method makes boxes smaller and also maintains feasible larger $g(\mathbf{b}^{(i)})$. The divided boxes satisfy the following conditions

$$\begin{aligned} \bigcup_{i=1, \dots, L+M} [\mathbf{a}^{(i)}, \mathbf{b}^{(i)}] &= [\mathbf{a}, \mathbf{b}] \setminus [\mathbf{p}, \mathbf{b}], \\ [\mathbf{a}^{(i)}, \mathbf{b}^{(i)}] \cap [\mathbf{a}^{(j)}, \mathbf{b}^{(j)}] &= \emptyset, \quad \forall i \neq j. \end{aligned} \quad (31)$$

Then, the box set \mathbb{S} is updated as following

$$\mathbb{S} = \mathbb{S} \setminus [\mathbf{a}, \mathbf{b}] \bigcup_{i=1, \dots, L+M} [\mathbf{a}^{(i)}, \mathbf{b}^{(i)}]. \quad (32)$$

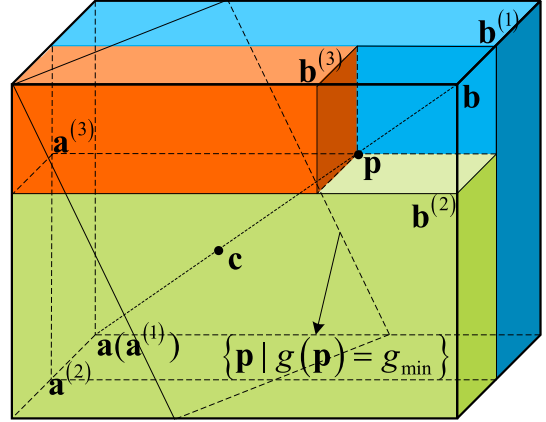


Fig. 4. Description of each iteration while $L + M = 3$.

From the set of boxes, it can be observed that the boxes contain some parts whose upper vertices cannot achieve higher objective values than the lower vertices. These boxes should be removed to guarantee that only feasible boxes are included. For each box $[\mathbf{a}, \mathbf{b}]$ of \mathbb{S} , if $g(\mathbf{b}) < g_{\min}$, this box is cut off from \mathbb{S} , otherwise, the lower vertex \mathbf{a} is reassigned as

$$a_i = b_i - \min \left(\frac{g(\mathbf{b}) - g_{\min}}{b_i - a_i}, 1 \right) \cdot (b_i - a_i). \quad (33)$$

The transformation of each iteration is illustrated in Fig. 4. At the end of each iteration, the upper vertices \mathbf{b} and the gap between \mathbf{a} and \mathbf{b} would decrease, and the whole iterative algorithm terminates while the gap is smaller than predefined tolerance.

Remark 2: Different from the outer polyblock approximation algorithm in [41], where polyblock always include whole achievable rate region, the box set \mathbb{S} in our algorithm only maintains the optimal solutions and thus can be reviewed as more efficient polyblock. Besides, the size of box would be shortened with iteration process, and the proposed algorithm will finally converge. The proposed monotonic algorithm is summarized in Algorithm 1.

For checking the feasibility of vertices in step 16 of Algorithm 1, the problem can be converted into

$$\begin{aligned} &\max_{\mathbf{W}_s, \mathbf{W}_m} 0 \\ &\text{s.t. } \tilde{\mathcal{C}}1 - \tilde{\mathcal{C}}5. \end{aligned} \quad (34)$$

However, the non-convex rank-1 constraint $\tilde{\mathcal{C}}5$ makes the problem (34) untractable. Different from the commonly used semi-definite programming (SDP) relaxation, which is not suitable to solving the non-convex constraints, we adopt the iterative penalty function (IPF) approach and rewrite the non-convex constraint $\tilde{\mathcal{C}}5$ as

$$\text{Tr}(\mathbf{W}_i) - \lambda_{\max}(\mathbf{W}_i) \leq 0, \quad \forall i \in \{s, 1, \dots, M\} \quad (35)$$

where $\lambda_{\max}(\mathbf{X})$ denotes the maximum eigenvalue of matrix \mathbf{X} . It should be mentioned that $\text{Tr}(\mathbf{W}_i) \geq \lambda_{\max}(\mathbf{W}_i)$ holds true for any \mathbf{X} , thus the constraint $\tilde{\mathcal{C}}5$ implies that $\text{Tr}(\mathbf{W}_i) = \lambda_{\max}(\mathbf{W}_i)$ and \mathbf{W}_i only has one nonzero eigenvalue, which can be expressed as

$$\mathbf{W}_i = \lambda_{\max}(\mathbf{W}_i) \mathbf{w}_{i \max} \mathbf{w}_{i \max}^H, \quad \forall i \quad (36)$$

Algorithm 1: The Proposed Monotonic Optimization Algorithm.

Input: $\{\mathbf{f}_{s,l}, \mathbf{f}_{a,m}, \mathbf{h}_{a,m}, \mathbf{h}_{s,l}\}$ and $\Gamma_{s,l}, \Gamma_{a,m}, P_{a,i}, P_{s,j}$.

- 1 Set the tolerance of accuracy ε_1 and line search accuracy δ ;
- 2 Calculate $\mathbf{a}_0, \mathbf{b}_0$ and initialize $g_{\max} = g(\mathbf{b}_0), g_{\min} = g(\mathbf{a}_0)$;
- 3 **while** $g_{\max} - g_{\min} > \varepsilon_1$ **do**
- 4 Set $state = 0$;
- 5 **repeat**
- 6 Choose a box $[\mathbf{a}, \mathbf{b}]$ from \mathbb{S} with $g(\mathbf{b}) = g_{\max}$;
- 7 Check the feasibility of \mathbf{a} ;
- 8 **if** feasible **then**
- 9 $state = 1$;
- 10 **else**
- 11 Set $\mathbb{S} = \mathbb{S}/[\mathbf{a}, \mathbf{b}]$;
- 12 $g_{\max} = \max_{\mathbb{S}} g(\mathbf{b})$;
- 13 **end**
- 14 **until** $state = 1$;
- 15 Set $\mathbf{c} = \mathbf{a} + (\mathbf{b} - \mathbf{a}) \cdot \frac{g_{\min} - g(\mathbf{a})}{g(\mathbf{b} - \mathbf{a})}$;
- 16 Check the feasibility of \mathbf{c} ;
- 17 **if** feasible **then**
- 18 Search for the intersection point along l_{ab} to obtain \mathbf{p} ;
- 19 Set $g_{\min} = g(\mathbf{p})$;
- 20 **else**
- 21 **end**
- 22 Divide the box $[\mathbf{a}, \mathbf{b}]$ into $L + M$ new boxes by (28) and (29) ;
- 23 Update \mathbb{S} through (31) ;
- 24 **for** any $[\mathbf{a}, \mathbf{b}] \in \mathbb{S}$ **do**
- 25 **if** $g(\mathbf{b}) > g_{\min}$ **then**
- 26 Reassign the upper vertex \mathbf{a} by (32) ;
- 27 **else**
- 28 Update $\mathbb{S} = \mathbb{S} \setminus [\mathbf{a}, \mathbf{b}]$;
- 29 **end**
- 30 **end**
- 31 Set $g_{\max} = \max_{\mathbb{S}} g(\mathbf{b})$;
- 32 **end**
- 33 Set $\{\Gamma_{s,l}, \Gamma_{a,m}\} = \mathbf{a}$;
- 34 Use singular value decomposition (SVD) to $\mathbf{V}^{(l)}$ and $\mathbf{W}_m^{(l)}$ to yield \mathbf{w}_s and $\mathbf{w}_{m,k}$;

Output: Optimal beamforming vectors $\mathbf{w}_s, \mathbf{w}_m$.

where $\mathbf{w}_{i,\max}$ is the corresponding eigenvector of maximum eigenvalue. The problem (34) can be reformulated as

$$\begin{aligned} & \max_{\mathbf{W}_s, \mathbf{W}_m} 0 \\ \text{s.t. } & \text{Tr}(\mathbf{W}_i) - \lambda_{\max}(\mathbf{W}_i) \leq 0, \quad \forall i \\ & \tilde{C}1-\tilde{C}4. \end{aligned} \quad (37)$$

Since $\text{Tr}(\mathbf{W}_i)$ is a linear function of \mathbf{W}_i , and $\lambda_{\max}(\mathbf{W}_i)$ is also convex on \mathbf{W}_i , leading (35) to a reverse convex constraint. It is worth mentioning that if $\text{Tr}(\mathbf{W}_i) - \lambda_{\max}(\mathbf{W}_i)$ is small enough, $\text{Tr}(\mathbf{W}_i)$ can be approximated as

Algorithm 2: The Proposed IPF Algorithm.

Input: $\{\mathbf{f}_{s,l}, \mathbf{f}_{a,m}, \mathbf{h}_{a,m}, \mathbf{h}_{s,l}\}$ and $r_{s,l}, r_{a,m}, P_{a,i}, P_{s,j}$.

- 1 Set the tolerance of accuracy ε_2 ;
- 2 Initialize the algorithm with feasible solution $\mathbf{W}_s, \mathbf{W}_m$;
- 3 Set the iteration number $l = 0$, weight $\eta > 0$;
- 4 **while** Problem (40) is feasible & $|\text{Tr}(\mathbf{W}^{(l)}) - \lambda_{\max}(\mathbf{W}^{(l)})| > \varepsilon_2$ **do**
- 5 Solve the problem (40);
- 6 Obtain solutions $\mathbf{W}, \alpha_{m,k}$ and set $\mathbf{W}^{(l+1)} := \mathbf{W}$;
- 7 **if** $\mathbf{W}^{(l+1)} \approx \mathbf{W}^{(l)}$ **then**
- 8 Set $\eta := 2\eta$;
- 9 **else**
- 10 Set $l := l + 1$;
- 11 **end**
- 12 **end**

Output: Beamforming weight matrices \mathbf{W}_s and $\mathbf{W}_{m,k}$.

$\lambda_{\max}(\mathbf{W}_i)\mathbf{w}_{i,\max}\mathbf{w}_{i,\max}^H$. Accordingly, our objective is to make $\text{Tr}(\mathbf{W}_i) - \lambda_{\max}(\mathbf{W}_i)$ as small as possible. By employing a penalty function method to substitute the constraint (36) into the objective function in (37), we obtain

$$\begin{aligned} & \max_{\mathbf{W}_s, \mathbf{W}_m} -\eta_s \text{Tr}(\mathbf{W}_s - \lambda_{\max}(\mathbf{W}_s)) \\ & \quad - \sum_{m=1}^M \eta_m \text{Tr}(\mathbf{W}_m - \lambda_{\max}(\mathbf{W}_m)) \\ \text{s.t. } & \tilde{C}1-\tilde{C}4 \end{aligned} \quad (38)$$

where η_i is a weight large enough to guarantee the small value of $\text{Tr}(\mathbf{W}_i) - \lambda_{\max}(\mathbf{W}_i)$. Obviously, the objective function in (38) is concave, thus (38) is a maximization problem of a concave function over convex constraints, which belongs to the class of concave programming. Besides, note that $\lambda_{\max}(\mathbf{W}_i)$ is nonsmooth, by exploiting the subgradient version of the maximal eigenvalue function $\partial\lambda_{\max}(\mathbf{X}) = \mathbf{x}_{\max}\mathbf{x}_{\max}^H$, we have

$$\lambda_{\max}(\mathbf{X}) - \lambda_{\max}(\mathbf{W}_i) = \langle \mathbf{w}_{i,\max}\mathbf{w}_{i,\max}^H, \mathbf{X} - \mathbf{W}_i \rangle. \quad (39)$$

As a result, by initializing the feasible points $\mathbf{W}_i^{(l)}$ of \mathbf{W}_i and the maximal eigenvalue and corresponding eigenvector of $\mathbf{W}_i^{(l)}$, the problem (39) can be rewritten as

$$\begin{aligned} & \max_{\mathbf{W}_s, \mathbf{W}_m} -\eta_s \left(\text{Tr}(\mathbf{W}_s) - \left\langle \mathbf{w}_s^{(l)} \left(\mathbf{w}_s^{(l)} \right)^H, \mathbf{W}_s \right\rangle \right) \\ & \quad - \sum_{m=1}^M \eta_m \left(\text{Tr}(\mathbf{W}_m) - \left\langle \mathbf{w}_m^{(l)} \left(\mathbf{w}_m^{(l)} \right)^H, \mathbf{W}_m \right\rangle \right) \\ \text{s.t. } & \tilde{C}1-\tilde{C}4. \end{aligned} \quad (40)$$

By assuming the optimal solution of (40) is $\mathbf{W}_i^{(l+1)}$, it can be verified that the iterative problem (40) is convergent as (41) shown at the bottom of the next page, which validate the iterative procedure, and the IPF algorithm is illustrated in Algorithm 2.

To solve P2 to obtain f_2^* , since both the objective (minimization of transmit power) and constraints $\tilde{C}1-\tilde{C}5$ are linear and convex, which can be efficiently solved by software

package, such as CVX. Thus, the process is omitted for simplification.

After obtaining the optimal objective value of P1 and P2, by introducing a variable τ , the MOO problem P3 can be expressed as

$$\begin{aligned} & \min_{\mathbf{W}_s, \mathbf{W}_m} \tau \\ & \text{s.t. } \tilde{\text{C}}1 - \tilde{\text{C}}5, \end{aligned}$$

$$\text{C6: } \lambda_n(f_n(\mathbf{v}, \mathbf{w}_m) - f_n^*) \leq \tau, \quad \forall n = \{1, 2\}. \quad (42)$$

It can be found that when $n = 2$, the constraint C6 is convex due to the linear structure of power minimization. When $n = 1$, by introducing variables $\mathbf{t} = \{t_{s,1}, \dots, t_{s,L}, t_{a,1}, \dots, t_{a,M}\}$ to represent achievable rate of ESs and MTs, the problem (41) can be rewritten as

$$\begin{aligned} & \min_{\mathbf{W}_s, \mathbf{W}_m, t_{s,l}, t_{a,m}} \tau \\ & \text{s.t. } \tilde{\text{C}}1 - \tilde{\text{C}}4, \\ & \quad \lambda_1 \left(\sum_{m=1}^M t_{a,m} + \sum_{l=1}^L t_{s,l} - f_1^* \right) \leq \tau, \\ & \quad \log_2(1 + \gamma_{a,m}) \leq t_{a,m}, \quad \forall m, \\ & \quad \log_2(1 + \gamma_{s,l}) \leq t_{s,l}, \quad \forall l, \\ & \quad \lambda_2 \left(\text{Tr}(\mathbf{W}_s) + \sum_{m=1}^M (\mathbf{W}_m) - f_2^* \right) \leq \tau. \quad (43) \end{aligned}$$

The above problem can be efficiently solved by Algorithm 1 and Algorithm 2, which is omitted here for brevity.

V. NUMERICAL RESULTS

This section provides simulation results for evaluating the performance of the proposed robust beamforming scheme in ISHAPN. Here, we consider a scenario of $L = 3$ ESs, and $M = 3$ MTs. For simplicity, we set the weighted factor of user rate as $\alpha_{s,l} = \alpha_{a,m} = 1/(L+M)$, the SINR threshold of ESs and MTs as $\Gamma_{a,m} = \Gamma_{s,l} = 3$ dB, and the tolerance of accuracy $\varepsilon_1 = \varepsilon_2 = 10^{-4}$. Other parameters are listed in Table II. We compare the performance of the proposed BF scheme with the other three schemes:

- The “SCA-based BF scheme” was proposed in [42], where the authors adopted SCA method to transform the sum

TABLE II
MAIN SIMULATION PARAMETERS

Parameter	Value
Orbit	GEO
Carrier frequency	18 GHz
Number of satellite antennas	$N_s = 7$
Maximal beam gain	$G_{\max} = 52$ dB
Rain fading	$\mu = -3.125, \sigma = 1.591$
HAP height	20 km
3 dB angle	$\varphi_x^{3\text{dB}} = 60^\circ, \varphi_y^{3\text{dB}} = 10^\circ$
Antenna inter-element spacing	$d_1 = d_2 = \lambda/2$
Side-lobe level	$S_m = 20$ dB
Number of NLoS paths	$L_n = 5$
Bandwidth	$B = 500$ kHz
Noise temperature	$T = 300$ K

secrecy rate maximization problem into a convex iterative problem.

- The “Zero-forcing BF scheme” and “MRT BF scheme” were adopted in [34], where the received signals are strengthened at intended user while nulled at unintended users in zero-forcing (ZF) BF scheme and the signals are directly toward intended user in MRT BF scheme.

Fig. 5(a) and Fig. 5(b) depict the beampatterns of the BF weight vector of our proposed robust BF scheme toward the 2nd MT from 3D vision and vertical vision. Note that the angular information based coordinate system is converted into geographic coordinate system for better intuitive understanding. It is assumed that HAP is deployed with 8×8 UPA, per-antenna power constraints are set as $P_{a,i} = P_{s,j} = 10$ dBmW, and the channel uncertainty region is set as $\Delta = 4^\circ$. Clearly, the maximal direction of BF weight vector points to the 2nd MT, and the received SINR at uncertainty region of the 2nd MT are guaranteed about -5 dB, while five nulls are generated with at least -60 dB at uncertainty region of other MTs and ESs, respectively, verifying that the obtained BF weight vectors of proposed robust BF scheme can efficiently improve the received signal quality at the intended user and simultaneously suppress the interference leakage at unintended users among the channel uncertainty region.

Fig. 6 plots the weighted sum rate of the considered system versus the per-antenna power constraint of HPA for different

$$\begin{aligned} F(\mathbf{W}_s^{(l+1)}, \mathbf{W}_m^{(l+1)}) &= -\eta_s \left(\text{Tr}(\mathbf{W}_s^{(l+1)}) - \lambda_{\max}(\mathbf{W}_s^{(l+1)}) \right) - \sum_{m=1}^M \eta_m \left(\text{Tr}(\mathbf{W}_m^{(l+1)}) - \lambda_{\max}(\mathbf{W}_m^{(l+1)}) \right) \\ &= -\eta_s \left(\text{Tr}(\mathbf{W}_s^{(l+1)}) - \lambda_{\max}(\mathbf{W}_s^{(l)}) - \left\langle \mathbf{w}_s^{(l)} \left(\mathbf{w}_s^{(l)} \right)^H, \mathbf{W}_s^{(l+1)} - \mathbf{W}_s^{(l)} \right\rangle \right) \\ &\quad - \sum_{m=1}^M \eta_m \left(\text{Tr}(\mathbf{W}_m^{(l+1)}) - \lambda_{\max}(\mathbf{W}_m^{(l)}) - \left\langle \mathbf{w}_m^{(l)} \left(\mathbf{w}_m^{(l)} \right)^H, \mathbf{W}_m^{(l+1)} - \mathbf{W}_m^{(l)} \right\rangle \right) \\ &\geq -\eta_s \left(\text{Tr}(\mathbf{W}_s^{(l)}) - \lambda_{\max}(\mathbf{W}_s^{(l)}) \right) - \sum_{m=1}^M \eta_m \left(\text{Tr}(\mathbf{W}_m^{(l)}) - \lambda_{\max}(\mathbf{W}_m^{(l)}) \right) \\ &= F(\mathbf{W}_s^{(l)}, \mathbf{W}_m^{(l)}) \end{aligned} \quad (41)$$

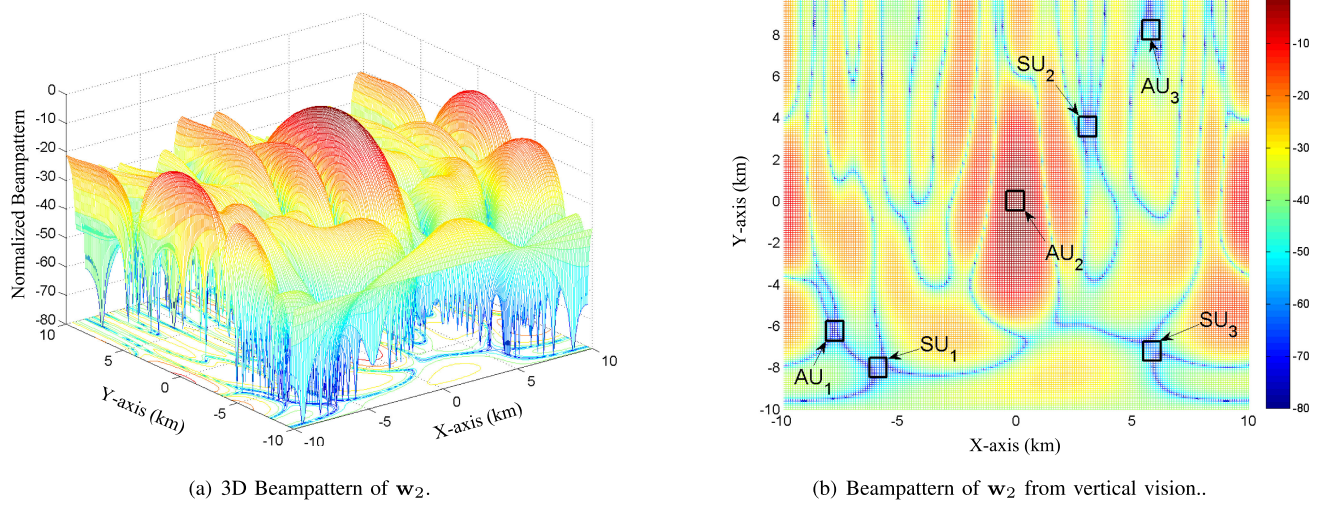
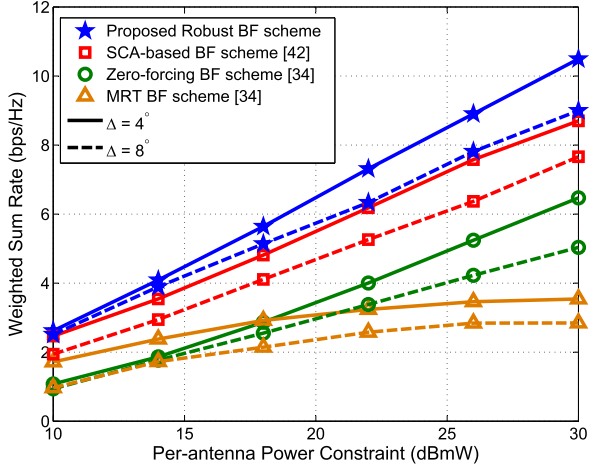
Fig. 5. Beampattern of w_2 in coordinate system.

Fig. 6. Weighted sum rate versus per-antenna power of HAP.

schemes. Here, the weighted factor of multi-objective problem is set as $\lambda_1 = 0.5$, the HAP is equipped with $N_b = 4 \times 4$ antennas and $P_{ant} = P_{a,i} = P_{s,j}$. It can be observed that the weighted sum rate of the proposed robust BF scheme increases linearly as the per-antenna power budget increases. When $P_{ant} = 22$ dBmW and channel uncertainty region $\Delta = 4^\circ$, the proposed robust BF scheme is enhanced by about 1.5, 3.5 and 4 bps/Hz in comparison with SCA-based BF scheme, ZF beamforming scheme and MRT beamforming scheme, respectively. Besides, when channel uncertainty region increases, the proposed robust BF maintains a stable performance compared to other three schemes.

Fig. 7 depicts the total transmit power versus the SINR threshold of MT $\Gamma_{a,m}$. Without loss of generality, we assume HAP is deployed with 4×4 UPA, $\Gamma_{s,l} = 3$ dB, $P_{a,i} = P_{s,j} = 10$ dBmW, the other parameters are similar to those in Fig. 6. Obviously, the proposed robust BF scheme always outperforms other schemes, verifying the superiority of our proposed scheme on enhancing the system performance. It can also be found that the total transmit power of the proposed robust scheme increases as SINR threshold $\Gamma_{a,m}$ increases. This is because while $\Gamma_{a,m}$

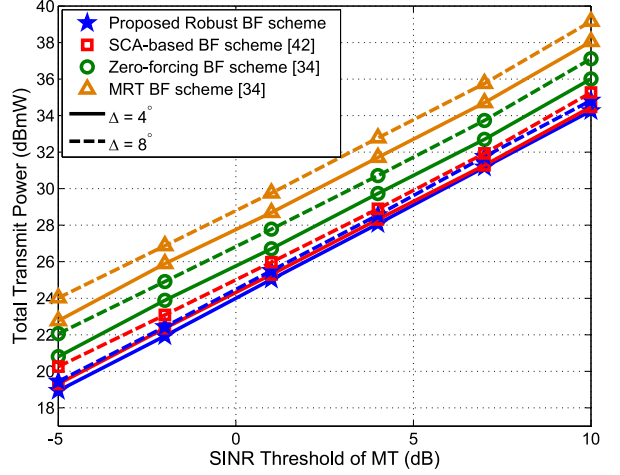


Fig. 7. Total transmit power versus SINR threshold of MT.

increases, the performance of MT should be improved, and thus the transmit power of HAP is also enlarged. In addition, the influence of channel uncertainty region on total transmit power is less than weighted sum rate in Fig. 6, the reason is that the SINR threshold is lower than the objective in Fig. 6, and the imperfect CSI has more effect on problem 1.

Fig. 8 depicts the trade-off region for weighted sum rate maximization and total transmit power minimization of the four schemes. As shown, the curve is obtained by varying the values of $\lambda_i \geq 0$ by the step of 0.1 subject to $\lambda_1 + \lambda_2 = 1$ to achieve the two objectives. We assume that HAP is deployed with 4×4 UPA, per-antenna power constraint $P_{a,i} = P_{s,j} = 10$ dBmW, and the channel uncertainty region $\Delta = 4^\circ$. It can be found that the weighted sum rate can be increased with a higher total transmit power. The Pareto boundary is obtained, which demonstrates that the two conflicting problems are partially aligned. As expected, our proposed robust BF method takes the channel uncertainty region into account, and thus outperforms the other three schemes. In particular, the performance gap between the proposed robust BF scheme and the non-robust schemes gets larger with an increased total transmit power.

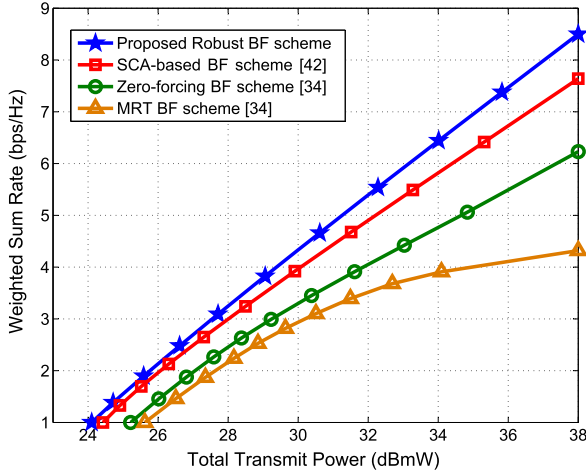


Fig. 8. Weighted sum rate versus total transmit power with different schemes.

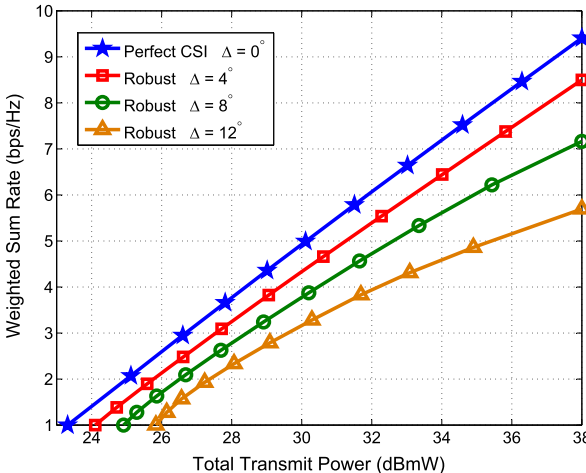


Fig. 9. Weighted sum rate versus total transmit power with different Δ .

Besides, the performance of the MRT beamforming scheme is worse than other schemes because it ignores the mutual interference between users, leading to less performance gain.

Fig. 9 presents the Pareto optimal boundary of the weighted sum rate maximization and total transmit power minimization with our proposed robust BF scheme based on various channel uncertainty regions. The parameters are similar with those in Fig. 8. As expected, the larger channel uncertainty region is, the worse Pareto optimal boundary obtained. Roughly speaking, the performance of the trade-off between the conflicting problems becomes better with a smaller channel uncertainty region. It can also be observed, while channel uncertainty region becomes larger, more transmit power would be consumed to maintain the improvement of weighted sum rate.

Furthermore, Fig. 10 and Fig. 11 illustrate the weighted sum rate and total transmit power against the antenna number of HAP, respectively. From Fig. 10, it can be seen that the weighted sum rate increases with increasing the antenna number, especially when the number of antennas is increased from 4×4 to 8×8 . It can also be observed that the weighted sum rate of ZF beamforming scheme and MRT beamforming scheme would converge gradually as the antenna number grows. The reason is that employing more antennas can simultaneously increase the

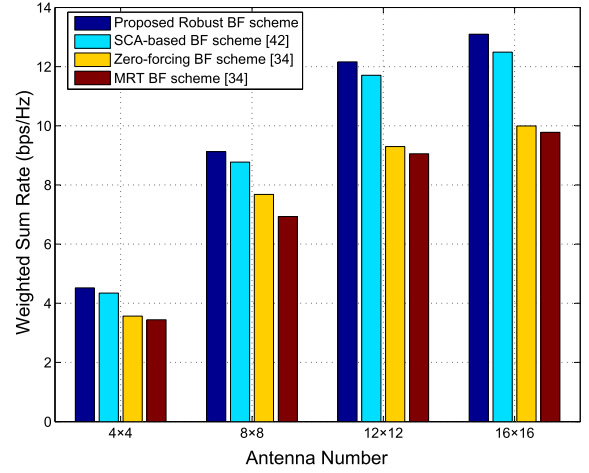


Fig. 10. Weighted sum rate versus antenna number of HAP.

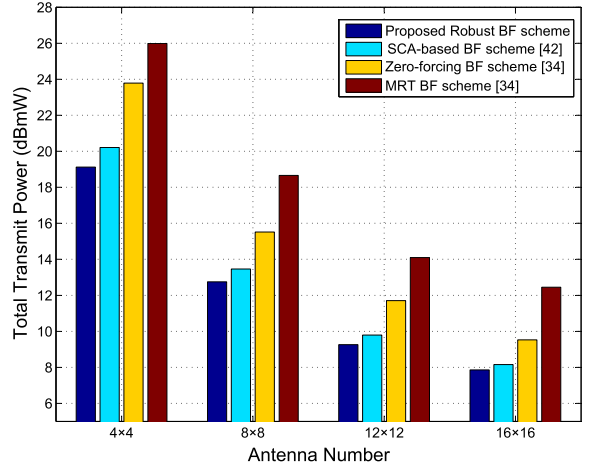


Fig. 11. Total transmit power versus antenna number of HAP.

intended signal strength and the inter-user interference strength, thus the weighted sum rate would converge to a constant value. Besides, as the antenna number increases from 4×4 to 12×12 , the difference in weighted sum rate between the proposed robust BF scheme and other three schemes becomes larger, indicating that increasing antenna number can enhance the advantage of our proposed robust scheme to a certain degree. From Fig. 11, the total transmit power decreases as antenna number increases, which is particularly transparent when the antenna number is increased from 4×4 to 8×8 . Furthermore, it is observed that the performance gap of total transmit power between schemes decrease with increasing of the array antenna number, this is because increasing antenna number can significantly improve the degree-of-freedom and diversity, which leads to less transmit power consumption and larger antenna amplifier energy, thus eventually decrease the performance gap.

VI. CONCLUSION

In this paper, we have investigated the robust BF design in the ISHAPN operating at mmWave band. By taking realistic scenario into account, we have assumed that only angular information based imperfect CSI can be obtained at transmitters. To investigate the trade off between the weighted sum rate maximization problem and the total transmit power minimization

problem, we have adopted the weighted Tchebycheff method to formulate the MOO problem, while satisfying the constraint of per-antenna transmit power and QoS of both satellite and HAP users. Since the formulated MOO problem is non-convex and mathematically intractable, we have first proposed a low-complexity discretization method to transform the non-convex objective function and constraints to the convex ones. Then, we have presented a monotonic optimization scheme combining with an iterative penalty function approach to obtain the rank-1 BF weight vectors. Compared to the commonly used SCA-based scheme, the proposed robust BF scheme can achieve better performance. Finally, simulation results have validated the effectiveness and superiority of the proposed robust BF scheme.

REFERENCES

- [1] ITU-R, "Revised technical and operational parameters for typical IMT-2000 terrestrial systems using high altitude platform stations and CDMA radio transmission technologies," Int. Telecommun. Union Document, 8-1/307-E, 1999.
- [2] C. Jiang, X. Wang, J. Wang, H.-H. Chen, and Y. Ren, "Security in space information networks," *IEEE Commun. Mag.*, vol. 53, no. 8, pp. 82–88, Aug. 2015.
- [3] A. Mohammed, A. Mehmood, F.-N. Pavlidou, and M. Mohorcic, "The role of high-altitude platforms (HAPs) in the global wireless connectivity," *Proc. IEEE*, vol. 99, no. 11, pp. 1939–1953, Nov. 2011.
- [4] X. Cao, P. Yang, M. Alzenad, X. Xi, D. Wu, and H. Yanikomeroglu, "Airborne communication networks: A survey," *IEEE J. Sel. Areas Commun.*, vol. 36, no. 9, pp. 1907–1926, Sep. 2018.
- [5] V. W. S. Wong *et al.*, *Key Technologies for 5 G Wireless Systems*. Cambridge, U.K.: Cambridge Univ. Press, 2017.
- [6] 3rd Generation Partnership Project, "Study on NR to support non-terrestrial networks," 3rd Generation Partnership Project, Tech. Rep. 38.811, Nov. 2017. [Online]. Available: <https://portal.3gpp.org/desktopmodules/Specifications/SpecificationDetails.aspx?specificationId=3234>
- [7] "Technical and operational characteristics for the fixed service using high altitude platform stations in the frequency range 18–32 GHz," Int. Telecommun. Union, Geneva, Switzerland, ITU-R f.[9B/KaCHAPS], 2000.
- [8] S. Maleki *et al.*, "Cognitive spectrum utilization in Ka band multibeam satellite communications," *IEEE Commun. Mag.*, vol. 53, no. 3, pp. 24–29, Mar. 2015.
- [9] ABSOLUTE, "Aerial base stations with opportunistic links for unexpected & temporary events," Whitepaper. [Online]. Available: <http://www.absolute-project.eu/>
- [10] E. Cianca *et al.*, "Integrated satellite-HAP systems," *IEEE Commun. Mag.*, vol. 43, no. 12, pp. 33–39, Dec. 2005.
- [11] M. Lin, Z. Lin, W.-P. Zhu, and J.-B. Wang, "Joint beamforming for secure communication in cognitive satellite terrestrial networks," *IEEE J. Sel. Areas Commun.*, vol. 36, no. 5, pp. 1017–1029, May 2018.
- [12] Z. Lin, M. Lin, J. Ouyang, W.-P. Zhu, A. D. Panagopoulos, and M.-S. Alouini, "Robust secure beamforming for multibeam satellite communication systems," *IEEE Trans. Veh. Technol.*, vol. 68, no. 6, pp. 6202–6206, Jun. 2019.
- [13] X. Zhu, C. Jiang, L. Kuang, N. Ge, and J. Lu, "Non-orthogonal multiple access based integrated terrestrial-satellite networks," *IEEE J. Sel. Areas Commun.*, vol. 35, no. 10, pp. 2253–2267, Oct. 2017.
- [14] J. Du, C. Jiang, H. Zhang, X. Wang, Y. Ren, and M. Debbah, "Secure satellite-terrestrial transmission over incumbent terrestrial networks via cooperative beamforming," *IEEE J. Sel. Areas Commun.*, vol. 36, no. 7, pp. 1367–1382, Jul. 2018.
- [15] P. G. Sudheesh, M. Mozaffari, M. Magarini, W. Saad, and P. Muthuchidambaranathan, "Sum-rate analysis for high altitude platform (HAP) drones with tethered balloon relay," *IEEE Commun. Lett.*, vol. 22, no. 6, pp. 1240–1243, Jun. 2018.
- [16] M. D. Zakaria, D. Grace, and P. D. Mitchell, "Antenna array beamforming strategies for high altitude platform and terrestrial coexistence using K-means clustering," in *Proc. IEEE 13th Malaysia Int. Conf. Commun.*, 2017, pp. 259–264.
- [17] Y. Wang, X. Xia, K. Xu, Y. Xu, and A. Liu, "Location-assisted precoding for three-dimension massive MIMO in air-to-ground transmission," in *Proc. IEEE InfoCOM Workshop*, May 2017, pp. 337–342.
- [18] F. Zhou, Z. Li, J. Cheng, Q. Li, and J. Si, "Robust AN-aided beamforming and power splitting design for secure MISO cognitive radio with SWIPT," *IEEE Trans. Wireless Commun.*, vol. 16, no. 4, pp. 2450–2464, Apr. 2017.
- [19] G. Zheng, K.-K. Wong, and T.-S. Ng, "Robust linear MIMO in the downlink: A worst-case optimization with ellipsoidal uncertainty regions," *EURASIP J. Adv. Signal Process.*, 2008, pp. 1–15.
- [20] G. Zheng, K.-K. Wong, and B. Ottersten, "Robust cognitive beamforming with bounded channel uncertainties," *IEEE Trans. Signal Process.*, vol. 57, no. 12, pp. 4871–4881, Dec. 2009.
- [21] F. Zhou, Z. Chu, H. Sun, R. Q. Hu, and L. Hanzo, "Artificial noise aided secure cognitive beamforming for cooperative MISO-NOMA using SWIPT," *IEEE J. Sel. Areas Commun.*, vol. 36, no. 4, pp. 918–931, Apr. 2018.
- [22] J. Huang and A. L. Swindlehurst, "Robust secure transmission in MISO channels based on worst-case optimization," *IEEE Trans. Signal Process.*, vol. 60, no. 4, pp. 1696–1707, Apr. 2012.
- [23] G. Zheng, K.-K. Wong, A. Paulraj, and B. Ottersten, "Robust collaborative-relay beamforming," *IEEE Trans. Signal Process.*, vol. 57, no. 8, pp. 3130–3143, Aug. 2009.
- [24] B. Li, Z. Fei, Z. Chu, F. Zhou, K.-K. Wong, and P. Xiao, "Robust chance-constrained secure transmission for cognitive satellite-terrestrial networks," *IEEE Trans. Veh. Technol.*, vol. 67, no. 5, pp. 4208–4219, May 2018.
- [25] S. Ma, M. Hong, E. Song, X. Wang, and D. Sun, "Outage constrained robust secure transmission for MISO wiretap channels," *IEEE Trans. Wireless Commun.*, vol. 13, no. 10, pp. 5558–5570, Oct. 2014.
- [26] W. Shi and J. Ritcey, "Robust beamforming for MISO wiretap channel by optimizing the worst-case secrecy capacity," in *Proc. 44th IEEE Asilomar Conf. Signals, Syst., Comput.*, 2010, pp. 300–304.
- [27] Y. Xu, X. Xia, K. Xu, and Y. Wang, "Three-dimension massive MIMO for air-to-ground transmission: location-assisted precoding and impact of AoD uncertainty," *IEEE Access*, vol. 5, pp. 15582–15596, 2017.
- [28] Z. Lin, M. Lin, J.-B. Wang, Y. Huang, and W.-P. Zhu, "Robust secure beamforming for 5G cellular networks coexisting with satellite networks," *IEEE J. Sel. Areas Commun.*, vol. 36, no. 4, pp. 932–945, Apr. 2018.
- [29] E. Bjornson, E. A. Jorswieck, M. Debbah, and B. Ottersten, "Multi-objective signal processing optimization: The way to balance conflicting metrics in 5G systems," *IEEE Signal Process. Mag.*, vol. 31, no. 6, pp. 14–23, Jun. 2014.
- [30] B. Li, Z. Fei, S. Yang, C. Xing, H. Chen, and L. Hanzo, "A survey of multi-objective optimization in wireless sensor networks: Metrics, algorithms, and open problems," *IEEE Commun. Surv. Tut.*, vol. 19, no. 1, pp. 550–586, Jan.–Mar. 2017.
- [31] Y. Sun, D. W. K. Ng, J. Zhu, and R. Schober, "Multi-objective optimization for robust power efficient and secure full-duplex wireless communication systems," *IEEE Trans. Wireless Commun.*, vol. 15, no. 8, pp. 5511–5526, Aug. 2016.
- [32] D. W. K. Ng, E. S. Lo, and R. Schober, "Multiobjective resource allocation for secure communication in cognitive radio networks with wireless information and power transfer," *IEEE Trans. Veh. Technol.*, vol. 65, no. 5, pp. 3166–3184, May 2016.
- [33] Z. Li, S. Gong, C. Xing, Z. Fei, and X. Yan, "Multi-objective optimization for distributed MIMO networks," *IEEE Trans. Commun.*, vol. 65, no. 10, pp. 4247–4259, Oct. 2017.
- [34] Z. Lin, M. Lin, J. Ouyang, W.-P. Zhu, and S. Chatzinotas, "Beamforming for secure wireless information and power transfer in terrestrial networks coexisting with satellite networks," *IEEE Signal Process. Lett.*, vol. 25, no. 8, pp. 1166–1170, Aug. 2018.
- [35] A. M. K., "Channel estimation and detection in hybrid satellite-terrestrial communication systems," *IEEE Trans. Veh. Technol.*, vol. 65, no. 7, pp. 5764–5771, Jul. 2016.
- [36] S. D. Gray, "A nulling performance comparison between a single- and multiple-aperture multiple-beam antenna," *IEEE Trans. Antennas Propag.*, vol. 43, no. 11, pp. 1319–1324, Nov. 1995.
- [37] A. Young, M. V. Ivashina, R. Maaskant, O. A. Iupikov, and D. B. Davidson, "Improving the calibration efficiency of an array fed reflector antenna through constrained beamforming," *IEEE Trans. Antennas Propag.*, vol. 61, no. 7, pp. 3538–3545, Jul. 2013.
- [38] Guidelines for Evaluation of Radio Interface Technologies for IMT-Advanced, Document ITU-R M.2135, 2008.

- [39] H. Zhu and J. Wang, "Chunk-based resource allocation in OFDMA systems—Part I: Chunk allocation," *IEEE Trans. Commun.*, vol. 57, no. 9, pp. 2734–2744, Sep. 2009.
- [40] H. Zhu and J. Wang, "Chunk-based resource allocation in OFDMA systems—Part II: Joint chunk, power and bit allocation," *IEEE Trans. Commun.*, vol. 60, no. 2, pp. 499–509, Feb. 2012.
- [41] L. Liu, R. Zhang, and K. Chua, "Achieving global optimality for weighted sum-rate maximization in the K-user Gaussian interference channel with multiple antennas," *IEEE Trans. Wireless Commun.*, vol. 11, no. 5, pp. 1933–1945, May 2012.
- [42] Z. Lin, M. Lin, J. Wang, T. De Cola, and J. Wang, "Joint beamforming and power allocation for satellite-terrestrial integrated networks with nonorthogonal multiple access," *IEEE J. Sel. Topics Signal Process.*, vol. 13, no. 3, pp. 657–670, Jun. 2019.



Zhi Lin received the B.S. and M.S. degrees in information and communication engineering from the PLA University of Science and Technology, Nanjing, China, in 2013 and 2016, respectively. He is currently working toward the Ph.D. degree in electronic science and technology from the College of Communications Engineering, Army Engineering University of PLA, Nanjing, China. Since 2019, he has been a visiting student with the Department of Electrical and Computer Engineering, McGill University, Canada. His research interests include wireless communications, convex optimization, and array signal processing. He was the TPC member of many IEEE sponsored conferences, including IEEE International Conference on Communications, Globecom, Infocom, IEEE Vehicular Technology Conference, etc.



Min Lin (M'13) received the B.S. degree in electrical engineering from the National University of Defense Technology, Changsha, China, in 1993, the M.S. degree in electrical engineering from the Nanjing Institute of Communication Engineering, Nanjing, China, in 2000, and the Ph.D. degree in electrical engineering from Southeast University, Nanjing, China, in 2008. From April 2015 to October 2015, he has visited the University of California, Irvine, as a Senior Research Fellow. He is currently a Professor and supervisor of Ph.D. and graduate students with the Nanjing University of Posts and Telecommunications, Nanjing, China. He has authored or co-authored more than 130 papers. His current research interests include wireless communications and array signal processing. He has served as the Track Chair of Satellite and Space Communications of IEEE International Conference on Communications (ICC) in 2019, and a TPC member of many IEEE sponsored conferences, such as IEEE ICC and Globecom.



Yongming Huang (M'10–SM'17) received the B.S. and M.S. degrees from Nanjing University, Nanjing, China, in 2000 and 2003, respectively, and the Ph.D. degree in electrical engineering from Southeast University, Nanjing, China, in 2007. Since March 2007, he has been a faculty member with the School of Information Science and Engineering, Southeast University, where he is currently a Full Professor. During 2008–2009, he was visiting the Signal Processing Laboratory, Department of Electrical Engineering, Royal Institute of Technology (KTH), Stockholm, Sweden. He has authored/coauthored more than 200 peer-reviewed papers and holds more than 60 invention patents. His current research interests include MIMO wireless communications, millimeter wave wireless communications, and intelligent mobile communications. He has submitted around 20 technical contributions to IEEE standards, and was awarded a certificate of appreciation for outstanding contribution to the development of IEEE standard 802.11aj. He was an Associate Editor for the *IEEE TRANSACTIONS ON SIGNAL PROCESSING*, *IEEE WIRELESS COMMUNICATIONS LETTERS*, *EURASIP Journal on Advances in Signal Processing*, and *EURASIP Journal on Wireless Communications and Networking*, and a Guest Editor for the *IEEE JOURNAL SELECTED AREAS IN COMMUNICATIONS*.



Tomaso de Cola was born in Manosque, France, on April 28, 1977. He received the Laurea (Hons.) degree in telecommunication engineering, in 2001, the qualification degree as a Professional Engineer in 2002, and the Ph.D. degree in electronic and computer engineering, robotics, and telecommunications from the University of Genoa, Genoa, Italy, in 2010. From 2002 until 2007, he was with the Italian Consortium of Telecommunications, University of Genoa Research Unit, as a Scientist Researcher. Since 2008, he has been with the German Aerospace Centre (DLR), where he is involved in different European Projects focusing on different aspects of DVB standards, CCSDS protocols and testbed design. He is co-author of more than 80 papers, including international conferences and journals. His main research activity concerns: TCP/IP protocols, satellite networks, transport protocols for wireless links, interplanetary networks as well as delay tolerant networks. He has served on the technical program committee at several IEEE International Conferences and was the Guest Editor for *IEEE NETWORK*, *IEEE JOURNAL ON SELECTED AREAS IN COMMUNICATIONS*, and *IEEE WIRELESS COMMUNICATION MAGAZINE*. He currently serves as an Editor for the *IEEE COMMUNICATION LETTERS*, *Wireless Communication Letters*, and *Elsevier Computer Networks*. He is acting as a Chair of the Satellite and Space Communications technical committee within ComSoc, the Deputy-Area Director of the Space-Internetworking Services (SIS) within the CCSDS standardization body, as well as a Chair of the SatCom working group within the ETP Networld2020 platform.



Wei-Ping Zhu (SM'97) received the B.E. and M.E. degrees in electrical engineering from the Nanjing University of Posts and Telecommunications, Nanjing, China, and the Ph.D. degree in electrical engineering from Southeast University, Nanjing, China, in 1982, 1985, and 1991, respectively. He was a Postdoctoral Fellow from 1991 to 1992 and a Research Associate from 1996 to 1998 with the Department of Electrical and Computer Engineering, Concordia University, Montreal, Canada. During 1993–1996, he was an Associate Professor with the Department of Information Engineering, Nanjing University of Posts and Telecommunications. From 1998 to 2001, he worked with hi-tech companies in Ottawa, Canada, including Nortel Networks and SR Telecom, Inc. Since July 2001, he has been with Concordia's Electrical and Computer Engineering Department as a full-time faculty member, where he is currently a Full Professor. Since 2008, he has been an Adjunct Professor with the Nanjing University of Posts and Telecommunications, Nanjing, China. His research interests include digital signal processing fundamentals, speech and statistical signal processing, and signal processing for wireless communication with a particular focus on MIMO systems and cooperative communication. He was an Associate Editor for the *IEEE TRANSACTIONS ON CIRCUITS AND SYSTEMS PART I: FUNDAMENTAL THEORY AND APPLICATIONS* during 2001–2003, an Associate Editor for *Circuits, Systems, and Signal Processing* during 2006–2009, and an Associate Editor for the *IEEE TRANSACTIONS ON CIRCUITS AND SYSTEMS PART II: TRANSACTIONS BRIEFS* during 2011–2015. He was also a Guest Editor for the *IEEE JOURNAL ON SELECTED AREAS IN COMMUNICATIONS* for the special issues of: Broadband Wireless Communications for High Speed Vehicles, and Virtual MIMO during 2011–2013. He is currently an Associate Editor for the *Journal of the Franklin Institute*. He was the Secretary of Digital Signal Processing Technical Committee of the IEEE Circuits and System Society during June 2012–May 2014, and the Chair of the DSPTC during June 2014–May 2016.